Check for updates

EurJIC
European Journal of Inorganic Chemistry

Research Article
doi.org/10.1002/ejic.202500031

Chemistry Europe
European Chemical Societies Publishing

www.eurjic.org

Investigation of Pyrrolidinium-based Superoxides and Ozonides

Jonas R. Schmid,[a] Oliver R. H. Rennefeld,[a] Anja Wiesner,[a] Patrick Voßnacker,[a] Yan Lu,[a] Günther Thiele,[a] Johanna Schlögl,[a] Carsten Müller,[a] Martin Jansen,*[b] and Sebastian Riedel*[a]

Pyrrolidinium-based cations were systematically modified to investigate their influence on ozonide and superoxide anions and to understand the scattering of experimentally determined dimensions of these radical anions. Hence, 1-ethyl-1-methyl-pyrrolidinium, 1-propyl-1-methyl-pyrrolidinium and 1-butyl-1-methyl-pyrrolidinium superoxide, as well as 1-methyl-1-methyl-pyrrolidinium and 1-propyl-1-methyl-pyrrolidinium ozonide have been synthesized via ion exchange in liquid ammonia, and characterized by single-crystal X-ray diffraction. Attempts to crystallize the 1-ethyl-1-methyl-pyrrolidinium and 1-butyl-1-methyl-pyrrolidinium ozonide in the same way failed. Two fundamental causes for the variation in the dimensions of the radical anions were revealed: firstly, the reduced accuracy of the experimental data due to static disorder and increased thermal motion, and secondly, the effects of the environments to which the anions are exposed in the crystal matrix. Quantum-chemical calculations of the isolated or embedded anions were also performed, showing a significant influence of hydrogen bonding and crystal field effects.

Introduction

Ionic superoxides and ozonides constitute prominent classes of inorganic matter, and numerous reports have been published, addressing the first observations, confirmations of crystal structures, and determination of physical properties.[1] Still, the variations in the experimental O–O bond lengths and O–O–O bond angles, exceeding typical experimental error ranges of diffraction methods, continue to be an issue of concern. Tables 1 and 2 present a selection of reported O–O bond lengths and O–O–O bond angles, respectively, for ionic superoxides and ozonides as determined by single-crystal X-ray diffraction.

For $[NMe_3(C_6H_5)]O_2$[6] and $[NEt_3Me]O_3$[13] (bold lines in Tables 1 and 2), results from high-precision structure analyses yield O–O bond lengths for the O_2^- and O_3^- units of 133.2(2) pm and 133.4(2)/132.3(2) pm, respectively. In these structures, the anions do not seem affected much by disorder or thermal motion. However, the ranges for O–O bond lengths observed

Table 1. Experimentally determined dimensions of the superoxide anion. A specific example is highlighted in bold.

Compound	R(O–O)/pm	Reference
CsO_2 (Phase II, 293 K)	119	[2]
CsO_2 (*Pnam*, 20 K)	132.917(2)	[3]
$[1,3(NMe_3)_2\text{-}C_6H_4](O_2)_2 \cdot 3NH_3$	133.5(3), 134.5(3)	[4]
$[NMe_4]O_2 \cdot 3NH_3$	131.8(2)	[5]
$[PMe_4]O_2 \cdot 2NH_3$	131.5(5)	[5]
$[AsMe_4]O_2 \cdot 2NH_3$	132.0(3)	[5]
$[NMe_3(C_6H_5)]O_2$	**133.2(2)**	**[6]**
$[N(C_4H_9)_4]O_2 \cdot 2.5NH_3$	131.2(2)	[6]
$Cs_3(O_3)_2(O_2) \cdot NH_3$	123.1(6)	[7]

Table 2. Experimentally determined dimensions of the ozonide anion. A specific example is highlighted in bold.

Compound	R(O–O)/pm	∢(O–O–O)/°	Reference
NaO_3	135.3(3)	113.0(2)	[8]
α-RbO_3	133(2), 144(2)	108(2)	[9]
β-RbO_3	133.0(9), 134.1(8)	113.7(7)	[10]
α-CsO_3	133.3(9), 133.2(8)	114.6(6)	[11]
$[NMe_4]O_3$	128.8(3)	119.6(4)	[12]
$[NEt_3Me]O_3$	**133.4(2), 132.3(2)**	**116.7(1)**	**[13]**
$[N(C_8H_{16})_4]O_3 \cdot 1.5\ NH_3$	132(1), 132(2)	114.4(4)	[14]

[a] J. R. Schmid, O. R. H. Rennefeld, Dr. A. Wiesner, Dr. P. Voßnacker, Dr. Y. Lu, Dr. G. Thiele, J. Schlögl, Dr. C. Müller, Prof. Dr. S. Riedel
Anorganische Chemie, Institut für Chemie Biochemie
Freie Universität Berlin
Fabeckstraße 34/36
14195 Berlin,Germany
E-mail: s.riedel@fu-berlin.de

[b] Prof. Dr. Dr. M. Jansen
Max-Planck-Institut für Festkörperforschung
Heisenbergstraße 1
70569 Stuttgart, Germany
E-mail: m.jansen@fkf.mpg.de

Supporting information for this article is available on the WWW under https://doi.org/10.1002/ejic.202500031

© 2025 The Author(s). European Journal of Inorganic Chemistry published by Wiley-VCH GmbH. This is an open access article under the terms of the Creative Commons Attribution License, which permits use, distribution and reproduction in any medium, provided the original work is properly cited.

© 2025 The Author(s). European Journal of Inorganic Chemistry published by Wiley-VCH GmbH

Research Article
doi.org/10.1002/ejic.202500031

for other superoxides and ozonides (see supporting information (SI) Table S10 and Table S11 for an extended list of superoxide and ozonide structures), are conspicuously wide: 119 pm−135(5) pm[2] for O_2^- and 118.8(7) pm–144(2) pm[9,15] for O_3^-. Recent studies have revealed a particular sensitivity of these quantities towards crystal field effects[9] and hydrogen bonding.[13]

To further investigate this effect, we report the results of a systematic study on superoxides and ozonides of subtly varied pyrrolidinium cations. These are 1-methyl-1-methyl-pyrrolidinium abbreviated to $[MMP]^+$, 1-ethyl-1-methyl-pyrrolidinium $[EMP]^+$, 1-propyl-1-methyl-pyrrolidinium $[PMP]^+$ and 1-butyl-1-methyl-pyrrolidinium $[BMP]^+$, see Scheme 1.

For the cases considered here, we provide evidence that the variations in the O–O bond lengths and O–O–O bond angles observed are associated with (1) the respective environments, e.g., via hydrogen bonding to nearest neighbours in the solid, (2) artefacts resulting from the spatial-/time-averaging of X-ray diffraction methods, or both. For reference, we calculated the free anions in the gas phase at ROHF-CCSD(T), CASSCF, CASPT2, and DFT levels and performed unrelaxed surface scans along the O–O bond and the O–O–O angle at MRCI+Q and ROHF-CCSD(T) levels. Quantum-chemical benchmark calculations (Table S12 and Table S17) predict an O–O bond length of 136.3 pm and 136.2 pm for isolated O_2^- and O_3^-, respectively. In addition, unrelaxed surface scans along the O–O bond axis at the DFT level were also performed, including some packing effects through an embedding. Comparison of the latter computational results for bond lengths and bond angles and those found by X-ray diffraction enabled us to identify which of the factors mentioned above cause variations in the observed structures.

Results and Discussion

Syntheses and Crystal Growth of the Pyrrolidinium Superoxides and Ozonides

All superoxides and ozonides investigated were synthesized via ion exchange in liquid NH_3 from $[NMe_4]O_2$ or KO_3, respectively, and a specific ammonium cation loaded on an exchange resin. For a detailed description, see the experimental section. Crystals suitable for X-ray diffraction were grown by slowly cooling concentrated NH_3 or NH_3/H_2NMe solutions to −78 °C. Surprisingly, the ozonide and superoxide salts with the $[PMP]^+$ cation exhibited relatively high stability, whereas crystals of $[MMP]O_3{\cdot}NH_3$ spontaneously self-ignited even when only briefly warmed to room temperature (see S5.3.2.5 for the stability of the ozonide anion). Attempts to prepare crystals from further ozonides, e.g. $[EMP]O_3$ or $[BMP]O_3$ failed, as they showed too high solubility in all compatible solvents or remained as red oils after removal of the solvent (see Figure S7).

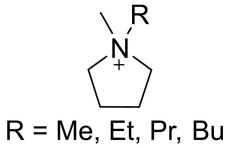

Scheme 1. Pyrrolidinium-based cations used during this investigation.

Crystal Structures of Superoxides

Crystal structures have been determined for the superoxides containing compounds $[EMP]O_2{\cdot}NH_3$, $[PMP]O_2$, and $[BMP]O_2{\cdot}EtOH$. In addition, the starting material, obtained in the shape of the solvent adduct $[NMe_4]O_2{\cdot}H_2NMe$ as a by-product during crystallization, was included. All bond lengths and angles of the ammonium cations and the solvent molecules found are in the realms as expected. Details on the determined structures are given in the SI Chapter S3. Here, only the ion pairs with the closest solvent molecules are displayed in Figure 1.

Investigation of the environment of the superoxide anions in the solids of $[NMe_4]O_2{\cdot}H_2NMe$, $[PMP]O_2$ and $[EMP]O_2{\cdot}NH_3$ revealed multiple hydrogen bonds O···H–C and O···H–N with O/H separations below the sum of van der Waals radii of hydrogen and oxygen (Chapter S3.3 and S3.4).[16] Steiner classifies these contacts as weak hydrogen bonds,[17] which would not be suited to induce the considerable contractions of the O–O bond lengths with respect to the equilibrium structure in vacuum, as observed by X-ray diffraction: 124.7(2) pm for $[NMe_4]O_2{\cdot}H_2NMe$, 126.9(3) pm for $[PMP]O_2$ and 118.0(2) pm for $[EMP]O_2{\cdot}NH_3$. These surprisingly short O–O bond lengths will be further discussed in the chapter on quantum-chemical investigations of superoxides.

In contrast, $[BMP]O_2{\cdot}EtOH$ also has weak O···H-(C) hydrogen bonds, but in addition one strong hydrogen bond between the

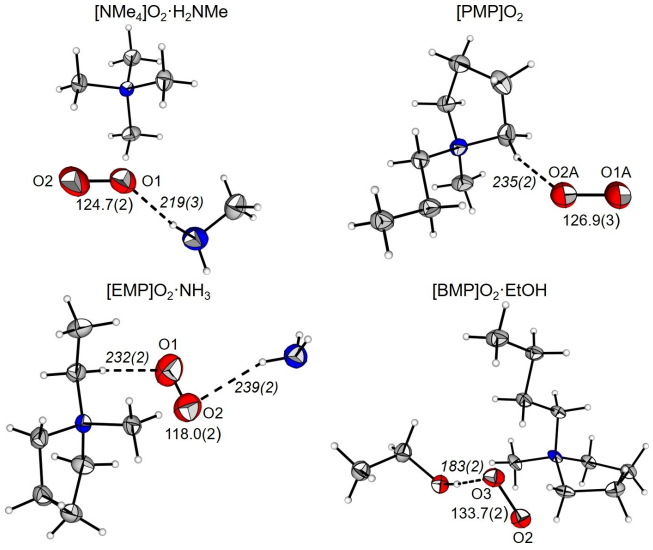

Figure 1. Cut outs from the crystal structure of $[NMe_4]O_2{\cdot}H_2NMe$, $[EMP]O_2{\cdot}NH_3$, $[PMP]O_2$ and $[BMP]O_2{\cdot}EtOH$. The shortest hydrogen bonds are highlighted as dotted lines and are given in italics in pm (for an extended list of hydrogen bond lengths and angles, see Table S3–S6). Bond lengths for the O–O bonds are given in pm. Thermal ellipsoids are set at 50% probability level. Hydrogen is white, nitrogen is blue, carbon is grey, and oxygen is red.

© 2025 The Author(s). European Journal of Inorganic Chemistry published by Wiley-VCH GmbH

Research Article
doi.org/10.1002/ejic.202500031

superoxide anion and the ethanol solvate molecule with an O···(H)-O distance of 266.1(1) pm (O···H-(O) distance of 183(2) pm), significantly below the combined van der Waals radii of oxygen and hydrogen at 262 pm.[16] Here, the intramolecular superoxide O–O bond appears to be of "regular length", due to the fixation of the superoxide anion via this strong hydrogen bond.

These findings, together with the trends in the Anisotropic Displacement Parameters (ADP) of the oxygen atoms (Table S9, high values highlighted in bold), offer a mode of explanation for the disparities of the superoxide O–O bond lengths observed. Librational thermal motion, as reflected by the ADPs, makes bond lengths appear shorter since the conventional tensor description of anisotropic thermal motion does not match librational motions.[18] For units consisting of at least four atoms, a TLS tensor analysis enables the extraction of realistic interatomic distances;[19] however, this approach fails for diatomic or triatomic entities.[20] As computational results presented in the next chapter will show, the short O–O bonds in $[NMe_4]O_2 \cdot H_2NMe$, $[PMP]O_2$, and $[EMP]O_2 \cdot NH_3$ are artefacts due to uncorrected enhanced thermal motion, see ADPs as bold numbers in Table S9. In $[BMP]O_2$·EtOH, however, the superoxide anion is involved in a hydrogen bond strong enough to hinder librational thermal motion, leading to low ADPs and a regular O–O bond length.

In addition to the effect discussed above, the by far too short O–O bond of 118.0(2) pm observed in the crystal structure of $[EMP]O_2 \cdot NH_3$ results also from experimental difficulties. The crystal studied was a two-domain twin, and the minute rotation by 1.3° of the minority against the main domain has impaired the twin integration (see Chapter S3.1). Because of the unsatisfactory precision for describing the O–O bond lengths, they are characterized by means of quantum-chemical calculations considering the chemical environment in the following chapter.

Quantum-Chemical Investigations of Superoxides

Optimizing the structure of an isolated superoxide anion yields an O–O bond length of about 135 pm (see Table S12). In experiment, the range of O–O bond lengths observed in superoxides was between 133 pm and 118 pm. Based on MRCI + Q(13/8)/ano-pVQZ calculations, such alterations of the bond length would require 2–88 kJ/mol, and it seems unlikely that this energy could be raised by the weak hydrogen bonds stabilizing the superoxide anion in the solid.

With a model derived from the $[BMP]O_2 \cdot$EtOH structure, containing the superoxide anion and the closest ethanol molecule, we calculated a binding energy corresponding to one hydrogen bond of −71 kJ/mol at the ROHF-CCSD(T)/aug-ano-pVTZ level in Molpro 2024.2 and −76 kJ/mol at the r^{2}SCAN-3c level in Orca 6.0.0. In order to estimate the bonding energy of all previously identified hydrogen bonds in the four systems shown in Figure 1 (see Tables S3-S6) and evaluate their influence on the superoxide's bond length, more advanced models with all molecules within a distance of $\leq$300 pm from the superoxide anion were used. A strong influence of the environment has already been demonstrated computationally for LiO_2 with the help of a solvent model.[21] For this larger model, CCSD(T) calculations were unfeasible, but the DFT method r^{2}SCAN-3c (meta-GGA composite method employing a modified def2-mTZVPP basis set) as implemented in Orca offered a reasonable compromise between performance and accuracy.

Within this model, the partial optimization of the superoxide's bond length yield values of 134–135 pm for all four systems (in good agreement with the results from Orca Docker Chapter S5.3.3), very close to the bond length in an isolated superoxide anion but much different from the value found by X-ray diffraction for e.g. $[EMP]O_2 \cdot NH_3$ (118 pm). Estimates for the strength of the hydrogen bonds in the four systems between the superoxide anion and the chemical environment were calculated from the potential energy density (V_{BCP}) at the corresponding bond critical points in the framework of QTAIM (quantum theory of atoms in molecules) analysis.[22] Indeed, the added bonding energies (see Table S16) are largest for the $[BMP]O_2 \cdot$EtOH system (with the smallest deviation of the O–O bond length from its equilibrium in the gas phase) and smallest for the $[EMP]O_2 \cdot NH_3$ system (with the largest shortening of the O–O bond length observed by X-ray diffraction).

As suggested earlier, the strengths of the hydrogen bonds in $[BMP]O_2$·EtOH appear to hinder the superoxide anion's thermal libration motion, which yields artificially too short O–O bond lengths in an analysis of the X-ray diffraction data. To investigate this further, a 2D potential energy scan with respect to rotations of the superoxide anion perpendicular to its main axis, as indicated in Figure 2, was performed (see Chapter S5.3.1.4). Indeed, this potential is steepest in the $[BMP]O_2 \cdot$EtOH system, limiting the libration of the superoxide anion to small angles. In the $[EMP]O_2 \cdot NH_3$ system, on the other hand, the potential is much flatter, allowing the superoxide anion to liberate much more due to thermal motion, resulting in apparently too short O–O bond lengths when analysing the X-ray diffraction data.

This approach could also be used for dioxygenyl salts to explain very short O–O bonds. $O_2[Hg(HF)]_4[SbF_6]_9$ may serve as an illustrative example, where very high ADP values and below-

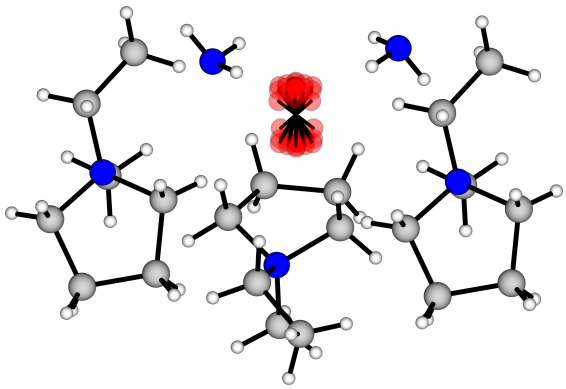

Figure 2. Exemplary representation of libration of O_2^- in $[EMP]O_2 \cdot NH_3$. Hydrogen is white, nitrogen is blue, carbon is grey, and oxygen is red.

© 2025 The Author(s). European Journal of Inorganic Chemistry published by Wiley-VCH GmbH

average O–O bond lengths indicate the presence of pronounced libration.[23]

Crystal structures of Ozonides

Syntheses and crystal growth of ozonides have been achieved only with the $[MMP]^+$ and $[PMP]^+$ cations. The ozonides based on $[EMP]^+$ and $[BMP]^+$ were obtained as dark red viscous oils, and it proved impossible to prepare single crystals within the respective thermal stability ranges (see Figure S7).

Details on the structure determinations are given as Supplementary Information (Chapter S3). The complex cations' interatomic distances and bond lengths are within the typical ranges. The ion pairs, and for $[MMP]^+$ also the closest solvent molecule, as cut-outs from the crystal structure, are shown in Figure 3. The ozonide anion in $[MMP]O_3 \cdot NH_3$ has significantly varying O–O bond lengths of 131.4(2) pm and 128.8(2) pm and an O–O–O angle of 118.9(2)°. Such a deviation of bond lengths in an ozonide anion is not unusual. However, it cannot be attributed to hydrogen bonds or other short contacts as seen from the Hirshfeld surfaces (Chapter S3.3.5). The longer O–O bond (131.4(2) pm) contains the terminal oxygen atom O1, which has only slightly weaker hydrogen bonds but in the same quantity as the other terminal oxygen atom O3. This contradicts the classical assumption that a strong hydrogen bond leads to an elongation of the corresponding hydrogen-bond-donor-substrate bond. Additional quantum-chemical analyses were carried out to exclude the possibility of intrinsic and extrinsic errors in the structure determination. These are discussed in the following chapter.

In contrast, $[PMP]O_3$ displays a more symmetrical ozonide anion with bond lengths of 133.0(2) pm and 134.2(2) pm and an angle of 116.08(9)°. Both terminal oxygen atoms are involved in three hydrogen bonds towards the surrounding cations. An additional hydrogen bond is formed at the central oxygen atom, which appears less favourable when considering the electrostatic potential mapped on the electron density map of the ozonide anion (Figure S28). Again, the shorter O–O bond (terminal oxygen O3) is involved in stronger hydrogen bonds.

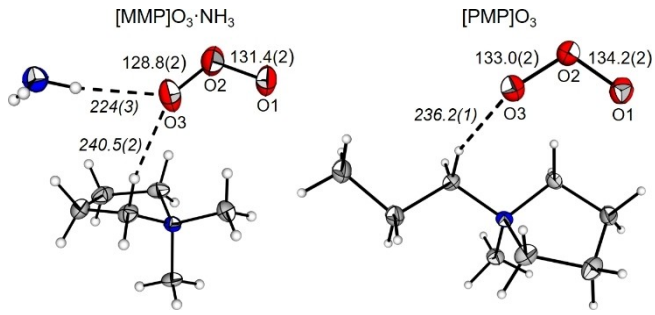

Figure 3. Cut outs of the crystal structure of $[MMP]O_3 \cdot NH_3$ and $[PMP]O_3$. The shortest hydrogen bonds are highlighted as dotted lines and are given in italics in pm (for an extended list of hydrogen bond lengths and angles, see Table S7-S8). Bond lengths for the O–O bonds are given in pm. The O–O–O bond angle for $[MMP]O_3 \cdot NH_3$ is 118.9(2)° and for $[PMP]O_3$ 116.08(9)°. Thermal ellipsoids are set at 50% probability level. Hydrogen is white, nitrogen is blue, carbon is grey, and oxygen is red.

These results may indicate that hydrogen bonds transfer electron density from the ozonide anion to the environment and thus reduce the antibonding character of the O–O bond. These values are in the range of those reported previously, see Table 2 and Table S11. Further studies on the packing motifs are given in SI (Figure S24-S25).

Quantum-Chemical Investigations of Ozonides

Optimizing the symmetric (C_{2v}) structure of an isolated ozonide anion yields an O–O bond length of 136 pm and a bond angle of 115° (see Table S17). From the crystallographically analysed ozonide structures, O–O bond lengths between 128.8(2) pm and 134.2(2) pm were observed and the anions deviated from C_{2v} symmetry. Based on ROHF-CCSD(T)/ano-pVQZ calculations, the energy loss for a distortion of the ozonide anion in reference to the optimised structure of the isolated anion was investigated for the ozonide anions in $[NMe_4]O_3$ (20 kJ/mol), $[MMP]O_3 \cdot NH_3$ (13 kJ/mol), Rb[18-crown-6]$O_3 \cdot NH_3$ (2 kJ/mol) and $[PMP]O_3$ (1 kJ/mol).[12,24] A similar distortion energy was observed for the ozonide anion in $[PMP]O_3$ assuming C_{2v} symmetry (2–4 kJ/mol for an O–O bond length of 133 pm or 134 pm) based on non-relaxed surface scans at MRCI + Q(13/8)/ano-pVQZ level of theory. These results (see also Chapter S5.3.2.1) show that the structure of an isolated ozonide anion can change significantly in terms of angle (±7.5°) and bond length (±7.5 pm) compared to the optimized structure without having to overcome a high energetic barrier.

This is in good agreement with previous studies and the solid-state dimensions of the ozonide anions in the high-resolution structures of $[C_6H_5CH_2NMe_3]O_3$, α-RbO_3 and $[N(C_4H_9)_4]O_3 \cdot 4.75NH_3$.[9,13,25] As for the superoxides, the chemical environment has a major influence on the radical anions and must also be considered. Therefore, $[MMP]O_3 \cdot NH_3$ and $[PMP]O_3$ were investigated with a similar embedded cluster model, including some nearest neighbours from the solid-state structure. A detailed description of the computational details can be found in Chapter S5.3.2.2. Partial structure optimizations of the embedded ozonide anion confirmed the asymmetry of the ozonide anion in $[PMP]O_3$ in the solid state. Although r^{2}SCAN-3c overestimates the ozonide's bond lengths by about 2 pm, the results indicate that the O–O bond lengths in $[MMP]O_3 \cdot NH_3$ are considerably misrepresented by X-ray diffraction and should be longer than observed. This observation is supported by high ADP values for the ozonide anion in $[MMP]O_3 \cdot NH_3$ (see Table S9). In addition, the crystal structure of $[NMe_4]O_3$ was investigated, which has O–O bond lengths that are too short for an ozonide anion and considerably high ADP values (see Table S20).[12] These results are in good agreement with the results from Orca Docker in Chapter S5.3.3. For the compounds $[PMP]O_3$ and $[MMP]O_3 \cdot NH_3$, the rotation of the ozonide anion was investigated in the same manner as for the superoxide compounds (see Figure 4). The calculations at the r^{2}SCAN-3c level of theory show that the rotational barriers correlate with the underestimation of O–O bond lengths by X-ray diffraction.

© 2025 The Author(s). European Journal of Inorganic Chemistry published by Wiley-VCH GmbH

Research Article
doi.org/10.1002/ejic.202500031

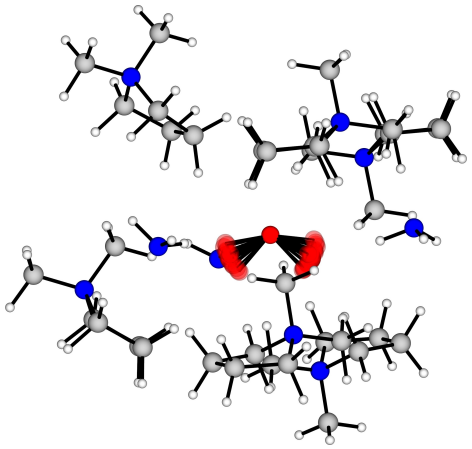

Figure 4. Exemplary representation of libration of O_3^- in $[MMP]O_3{\cdot}NH_3$. Hydrogen is white, nitrogen is blue, carbon is grey, and oxygen is red.

A similar estimation of the hydrogen bond strength based on AIM, as performed for the superoxides, yields accumulated interaction energies of −119 and −126 kJ/mol in $[PMP]O_3$ and $[MMP]O_3 \cdot NH_3$, respectively. Thus, the interaction of the environment with the ozonide anions is, in principle, stronger than with the superoxide anions. Despite the slightly larger interaction energy in $[MMP]O_3{\cdot}NH_3$, the ozonide anion appears to be a bit more influenced by libration, leading to larger underestimations of the O–O bond length than in $[PMP]O_3$. Here, the lower crystal quality of $[MMP]O_3 \cdot NH_3$ might have enlarged the observed shortening of the O–O bond lengths.

In general, the O–O bond lengths and O–O–O bond angles of the ozonide anion can be determined more reliably by X-ray diffraction due to the nonlinear symmetry and the higher tendency to form multiple interactions in the solid state, compared to the superoxide anion.

Vibrational Spectroscopy

The IR spectrum of $[PMP]O_2$ in comparison to [PMP]Cl is shown in Figure S1. A significant shift to lower wavenumbers (ca. 200 cm^{-1}) for the C–H stretching modes in $[PMP]O_2$ can be observed in comparison to [PMP]Cl. No single crystal Raman spectra could be obtained for the organic ozonides, due to decomposition induced by the excitation laser, even at 77 K (1064 nm laser). In the IR spectrum of $[MMP]O_3 \cdot NH_3$, two of the three ozonide-specific bands were observed at 779 cm^{-1} for the asymmetric stretching and at 542 cm^{-1} for the bending vibration. For $[PMP]O_3$, only the asymmetric stretching mode for the ozonide anion was observed at 778 cm^{-1} due to the complex cation spectrum. The full spectra and comparison to the spectra of their respective cations ([MMP]I and [PMP]Cl) as well as quantum-chemical calculations for the ozonide (BP86-D4/ano-pVQZ) are shown in Figure S2-S5.

Conclusions

In summary, the superoxide-containing compounds $[NMe_4]O_2 \cdot H_2NMe$, $[EMP]O_2 \cdot NH_3$, $[PMP]O_2$ and $[BMP]O_2{\cdot}EtOH$ have been synthesized and characterized by single-crystal X-ray diffraction. $[PMP]O_2$, a rare example of a superoxide compound without co-crystallized solvent molecules, was further characterized by IR spectroscopy and EPR measurements. In three of four systems, the thermal libration motion of the superoxide anion causes a systematic error in the X-ray diffraction analyses, feigning too short O–O bond lengths. The degree of libration is reflected in the ADP values and correlates with the strength of interaction between the superoxide anion and its environment through hydrogen bonds. Partial structure optimizations at the DFT level of embedded clusters were suitable for correcting the measured O–O bond lengths. Diffraction data obtained at lower temperatures would be suited to confirm this effect, as recently demonstrated for CsO_2, where the apparent O–O bond length seems to change drastically on cooling from 290 K (126.40 pm) to 20 K (132.91 pm).[3]

The ozonide-containing compounds $[MMP]O_3 \cdot NH_3$ and $[PMP]O_3$ were synthesized and characterized by single-crystal X-ray diffraction and IR spectroscopy. Here, the effect of thermal libration (reflected in high ADP values) leading to the prediction of O–O bond lengths that appear too short is also present but less pronounced. This hypothesis is supported by the higher ADP values for the ozonide anion in $[MMP]O_3 \cdot NH_3$, while a similar trend is shown for $[NMe_4]O_3$. Additionally, the ozonide-containing compounds $[EMP]O_3$ and $[BMP]O_3$ were studied. They show a very high solubility in all compatible solvents and an uncommon oily appearance.

Experimental Section

CAUTION! Strong Oxidizers!

Ozonides and superoxides are strong oxidizers that can lead to violent reactions with organic material. Strong friction can cause violent reactions. All reactions should be conducted under rigorously anhydrous conditions.

Materials, Chemicals and Procedures

All water and air-sensitive substances were handled under Argon (Ar 5.0) atmosphere using standard Schlenk techniques and a vacuum up to 10^{-3} mbar. If not mentioned otherwise, all syntheses were performed under the specified conditions. All glassware was flame-dried multiple times and joints were sealed with Triboflon grease. Specialised glassware used for the synthesis of the starting materials is shown in Figure S27. Ammonia (3.8 Linde) was dried by refluxing over NaK overnight, distilled, and stored in a dried stainless-steel gas cylinder. Single crystals were picked at −80 °C under a nitrogen atmosphere and mounted on a 0.15 mm Mitegen micromount using perfluoroether oil diluted with perfluorohexane. Crystal data were collected on a Bruker D8 Venture diffractometer with a Photon II area detector or Photon III area detector with CuKα or MoKα radiation at 100(1) K, 109(1), and 150(1) K. Multiscan absorption correction was used as implemented in APEX IV (SADABS-2016/2 or TWINABS).[26] The structures were solved with

© 2025 The Author(s). European Journal of Inorganic Chemistry published by Wiley-VCH GmbH

Research Article
doi.org/10.1002/ejic.202500031

the SHELXT[27] structure solution program using intrinsic phasing and refined with the SHELXL[28] refinement package using least squares minimizations by using OLEX2.[29] Hydrogen atoms were refined using HFIX 137 (CH_3) HFIX 23 ($C_{sp2}H$) as implemented. For visualization, the DIAMOND V4.65 program package was used.[30] IR spectra were recorded on a Nicolet iS50 Advance FTIR by Thermo Fisher Scientific equipped with an ATR unit, with a Ge on KBr beamsplitter and a DLaTGS-KBr detector for MIR and a solid-substrate beamsplitter with a DLaTGS-PE detector for FIR. For low-temperature measurements, a metal cylinder cooled by a cold N_2 stream was used. IR spectra were processed using OPUS 7.5,[31] OMNIC 9.7.46[32], and ORIGIN PRO 2022[33] was used for their graphical representation.

The EPR spectrum was recorded in the X-band at −196 °C with a Magnetech MS 5000 spectrometer. The sample was sealed in a 5 mm thick glass ampoule under an argon atmosphere. Simulations were performed with Easyspin.[34]

Quantum-chemical calculations were conducted using the HPC system provided by Freie Universität's IT-service FUB-IT.[35] The programs MOLPRO 2021.3 and MOLPRO 2024.2,[36] Orca 5.0.3, ORCA 5.0.4, ORCA 6.0.0[37] and GAUSSIAN 16[38] were used in combination with the B3LYP–D3(*BJ*),[39] BP86-D4,[39a,40] CCSD(T),[41] CASSCF,[42] MRCI + Q,[43] r^{2}SCAN-3c,[44] CASPT2[45] method and 6-311 + G-(3df,3pd), 6-311 + + G(3df,3pd), 6–311 + G(3df),[46] ano-pVTZ, ano-pVQZ, aug-ano-pVQZ,[47] aug-cc-pVTZ, aug-cc-pVQZ,[48] aug-cc-pwCVTZ[49] basis set. Overtones, combination bands, and ORCA DOCKER geometries were calculated using XTB 6.7.1.[50] Molecular orbitals were visualized using CHEMCRAFT 1.8.[51] Hirshfeld surfaces were visualized with CRYSTAL EXPLORER 21.5[52] and electronic potentials mapped onto electron densities were visualized with VMD 1.9.3.[53]

$[NMe_4]O_2$

Tetramethylammonium hydroxide pentahydrate (97 %, Acros) was dried to the monohydrate. The solid-state metathesis reaction between tetramethylammonium hydroxide monohydrate and potassium superoxide (thermo scientific) to obtain tetramethylammonium superoxide was carried out in a PFA round bottom flask analogous to the literature procedure, followed by the extraction with liquid ammonia.[54] Strong friction from a spatula can lead to ignition of the reaction mixture. The use of PFA reaction vessels can prevent adhesion to the surface of the devices, which means that the reaction mixture does not have to be removed from the surface by scraping.

KO_3

The compound was synthesized as described elsewhere.[55]

$[NMe_4]O_2 \cdot H_2NMe$

Single crystals suitable for x-ray diffraction could be obtained by suspending $[NMe_4]O_2$ in $MeNH_2$ at −33 °C and adding NH_3 until a clear solution was obtained. Single crystals were obtained by slowly cooling the reaction mixture to −77 °C.

$[EMP]O_2 \cdot NH_3$

The ion exchange resin Amberlyst® 15 (Merck) (3.0 g) was charged with 1-ethyl-1-methylpyrrolidin-1-ium (1-ethyl-1-methylpyrrolidin-1-ium chloride, IoLiTec, > 98 %) and was placed inside a H-shaped glass apparatus and cooled with a dry ice ethanol bath to −70 °C and $[NMe_4]O_2$ (ca. 150 mg, 1.41 mmol) was added. Afterwards, ammonia (ca. 10 mL) was condensed onto the solids at −196 °C and the mixture was allowed to warm to −33 °C to fully dissolve the superoxide. The solution was stored at −76 °C for 3 days and extracted 3 times as described before.[4] The pale-yellow solution was concentrated under vacuum at −60 °C, transferred in a Schlenk tube, concentrated again (> 1 mL), and crystallized at −77 °C.

$[PMP]O_2$

The ion exchange resin Amberlyst® 15 (Merck) (2.0 g) was charged with 1-methyl-1-propylpyrrolidin-1-ium (1-methyl-1-propylpyrrolidin-1-ium chloride, IoLiTec, > 98 %) and was placed inside a H-shaped glass apparatus and cooled with a dry ice ethanol bath to −70 °C and $[NMe_4]O_2$ (ca. 150 mg, 1.41 mmol) was added. Afterwards, ammonia (ca. 10 mL) was condensed onto the solids at −196 °C and the mixture was allowed to warm to −33 °C to fully dissolve the superoxide. The solution was stored at −76 °C for 3 days and extracted 5 times as described before.[4] The pale-yellow solution was concentrated under vacuum at −60 °C, transferred in a Schlenk tube, concentrated again (> 1 mL), and crystallized at −77 °C.

IR (ATR, −70 °C, 32 scans): $\tilde{\nu}$ = 3251 (m), 3196 (m), 3018 (m), 2966 (m), 2878 (m), 1599 (w), 1493 (s), 1474 (s), 1456 (s), 1337 (w), 1253 (w), 1060 (w), 1043 (w), 1029 (w), 1006 (m), 954 (s), 945 (s), 907 (w), 889 (w), 829 (w), 652 (s), 591 (s), 504 (w), 463 (w), 434 (w), 81 (w), 55 (s) cm^{-1}.

$[BMP]O_2 \cdot EtOH$

The ion exchange resin Amberlyst® 15 (Merck) (2.8 g) was charged with 1-butyl-1-methylpyrrolidin-1-ium (1-butyl-1-methylpyrrolidin-1-ium chloride, IoLiTec, > 98 %) and was placed inside a H-shaped glass apparatus and cooled with a dry ice ethanol bath to −70 °C and $[NMe_4]O_2$ (ca. 250 mg, 2.36 mmol) was added. Afterwards, ammonia (ca. 10 mL) was condensed onto the solids at −196 °C and the mixture was allowed to warm to −33 °C to fully dissolve the superoxide. The solution was stored at −76 °C for 3 days and extracted 3 times as described before.[4] The pale-yellow solution was concentrated under vacuum at −40 °C, transferred in a Schlenk tube, concentrated again (> 1 mL), and crystallized at −77 °C. Due to a leak, ethanol was able to enter the Schlenk tube from the cold bath and crystallized with the superoxide.

[MMP]I

1,1-dimethyl-1pyrrolidin-1-ium (48.2 g, 90 %) was synthesized in methanol instead of ethyl acetate according to a literature procedure.[56]

^{1}H NMR (401 MHz, DCM-d_2): δ = 3.71 (t, 4H), 3.34 (s, 6H), 2.17 (m, 4H) ppm. ^{13}C NMR (101 MHz, DCM-d_2): δ = 65.8 (t), 52.2 (t), 21.6 (s) ppm.

$[MMP]O_3 \cdot NH_3$

The ion exchange resin Amberlyst® 15 (Merck) (3.0 g) was charged with 1,1-dimethyl-1pyrrolidin-1-ium, placed inside a H-shaped glass apparatus and cooled with a dry ice ethanol bath to −70 °C. KO_3 (ca. 140 mg, 1.61 mmol) was added and ammonia (ca. 10 mL) was condensed onto the solids at −196 °C. The mixture was allowed to warm to −60 °C to fully dissolve the ozonide. The solution was stored at −76 °C for 3 days and extracted 3 times as described before.[25a] The red solution was concentrated under vacuum at −60 °C, transferred in a Schlenk tube, concentrated again (> 7 mL), and crystallized at −77 °C.

IR (ATR, −70 °C, 32 scans): $\tilde{\nu}$ = 3015 (w), 2970 (w), 2900 (w), 1769 (w), 1605 (w), 1477 (m), 1467 (m), 1419 (w), 1350 (w), 1306 (w), 1251 (w), 1227 (w), 1047 (w), 1000 (w), 978 (w), 936 (w), 779 (s, ν_{as} (O_3^-)), 580 (w), 542 (w, δ (O_3^-)), 433 (w), 257 (w), 60 (s) cm^{-1}.

$[PMP]O_3$

The ion exchange resin Amberlyst® 15 (Merck) (2.0 g) was charged with 1-methyl-1-propylpyrrolidin-1-ium (1-methyl-1-propylpyrrolidin-1-ium chloride, IoLiTec, > 98 %), placed inside a H-shaped glass

© 2025 The Author(s). European Journal of Inorganic Chemistry published by Wiley-VCH GmbH

apparatus and cooled with a dry ice ethanol bath to −70 °C. KO_3 (ca. 120 mg, 1.38 mmol) was added and ammonia (ca. 10 mL) was condensed onto the solids at −196 °C. The mixture was allowed to warm to −60 °C to fully dissolve the ozonide. The solution was stored at −76 °C for 4 days and extracted 3 times as described before.[25a] The red solution was concentrated under vacuum at −60 °C, transferred in a Schlenk tube, concentrated again (> 1 mL), and crystallized at −77 °C.

IR (ATR, −70 °C, 32 scans): $\tilde{\nu}$ = 3015 (w), 3006 (w), 2966 (m), 2934 (w), 2872 (w), 1766 (w), 1499 (w), 1478 (m), 1459 (w), 1435 (w), 1415 (w), 1379 (w), 1361 (w), 1340 (w),1307 (w), 1232 (w), 1152 (w), 1126 (w), 1051 (w), 1042 (w), 1010 (w), 976 (m), 949 (m), 943 (w), 907 (w), 778 (s, ν_{as} (O_3^-)), 586 (m), 444 (w), 87 (w), 66 (s), 52 (s) cm^{-1}.

Deposition Numbers CCDC: 2387898 for $[NMe_4]O_2{\cdot}H_2NMe$, 2387897 for $[EMP]O_2{\cdot}NH_3$, 2387901 for $[PMP]O_2$, 2387896 for $[BMP]O_2{\cdot}EtOH$, 2389098 for $[MMP]O_3{\cdot}NH_3$ and 2387902 for $[PMP]O_3$.

Supporting Information

The authors have cited additional references within the Supporting Information.[57–97]

Acknowledgements

We gratefully acknowledge the ERC Project HighPotOx (Grant agreement ID: 818862) and the Core Facility BioSupraMol supported by the DFG. We gratefully acknowledge the HPC unit of the IT-service (FUB-IT) at Freie Universität Berlin for the allocation of computing resources and user support. The authors like to thank Dirk Busold and Jesse Holloway for manufacturing the specialised glass apparatus. JRS thanks Dr. Paul Golz and Dr. Patrick Voßnacker for providing computation resources, Dr. Matthew Graneri for helpful discussions and Dr. Julia Bader for proofreading the Manuscript. Open Access funding enabled and organized by Projekt DEAL.

Conflict of Interests

The authors declare no conflict of interest.

Data Availability Statement

The data that support the findings of this study are available from the corresponding author upon reasonable request.

Keywords: Ozonide · Quantum Chemistry · Radical ions · Superoxide · X-ray diffraction

[1] a) S. A. Tokareva, *Russ. Chem. Rev.* **1971**, *40*, 165; b) W. Hesse, M. Jansen, W. Schnick, *Prog. Solid State Chem.* **1989**, *19*, 47; c) M. Jansen, H. Nuss, *Z. Anorg. Allg. Chem.* **2007**, *633*, 1307; d) H. Nuss, M. Jansen, *Ionic Ozonides – From Simple Inorganic Salts to Supermolecular Building Blocks in New Strategies Chemical Synthesis and Catalysis*, Wiley, Weinheim, **2012**, 79; e) M. Hayyan, M. A. Hashim, I. M. AlNashef, *Chem. Rev.* **2016**, *116*, 3029.
[2] M. Ziegler, M. Rosenfeld, W. Känzig, P. Fischer, *Helv. Phys. Acta* **1976**, *49*, 57.
[3] R. A. Ewings, M. Reehuis, F. Orlandi, P. Manuel, D. D. Khalyavin, A. S. Gibbs, A. D. Fortes, A. Hoser, A. J. Princep, M. Jansen, *Phys. Rev. B* **2023**, *108*, 174412.
[4] H. Seyeda, M. Jansen, *J. Chem. Soc. Dalton Trans.* **1998**, 875.
[5] P. D. C. Dietzel, R. K. Kremer, M. Jansen, *Chem. Asian J.* **2007**, *2*, 66.
[6] P. D. C. Dietzel, R. K. Kremer, M. Jansen, *J. Am. Chem. Soc.* **2004**, *126*, 4689.
[7] H. Nuss, M. Jansen, *Z. Anorg. Allg. Chem.* **2012**, *638*, 501.
[8] a) W. Klein, K. Armbruster, M. Jansen, *Chem. Commun.* **1998**, 707; b) W. Klein, M. Jansen, *Z. Anorg. Allg. Chem.* **2000**, *626*, 136.
[9] A. Sans, H. Nuss, S. Mohitkar, M. Jansen, *Z. Anorg. Allg. Chem.* **2017**, *643*, 357.
[10] W. Schnick, M. Jansen, *Z. Anorg. Allg. Chem.* **1986**, *532*, 37.
[11] M. Jansen, W. Assenmacher, *Z. Kristallogr.* **1991**, *194*, 315.
[12] W. Hesse, M. Jansen, *Inorg. Chem.* **1991**, *30*, 4380.
[13] J. R. Schmid, P. Voßnacker, M. Jansen, S. Riedel, *Z. Anorg. Allg. Chem.* **2022**, *648*, e202200225.
[14] W. Klein, *Diploma Thesis*, Univ. Bonn **1995**.
[15] H. Nuss, M. Jansen, *Angew. Chem. Int. Ed.* **2006**, *45*, 7969.
[16] A. Bondi, *J. Phys. Chem.* **1964**, *68*(3), 441.
[17] T. Steiner, *Angew. Chem. Int. Ed.* **2002**, *41*, 48.
[18] W. R. Busing, H. A. Levy, *Acta Crystallogr.* **1964**, *17*, 142.
[19] V. Schomaker, K. N. Trueblood, *Acta Crystallogr.* **1968**, *B24*, 63.
[20] C. Scheringer, *Acta Crystallogr.* **1972**, *A28*, 619.
[21] A. Zaichenko, D. Schröder, J. Janek, D. Mollenhauer, *Chem. Eur. J.* **2020**, *26*, 2395.
[22] E. Espinosa, E. Molins, C. Lecomte, *Chem. Phys. Lett.* **1998**, *285*, 170.
[23] Z. Mazej, E. Goreshnik, *Inorg. Chem.* **2020**, *59*, 2092.
[24] H. Nuss, J. Nuss, M. Jansen, *Z. Anorg. Allg. Chem.* **2008**, *634*, 1291.
[25] a) N. Korber, M. Jansen, *Chem. Ber.* **1992**, *125*, 1383; b) P. D. C. Dietzel, M. Jansen, *Z. Anorg. Allg. Chem.* **2006**, *632*, 2276.
[26] a) L. Krause, R. Herbst-Irmer, G. M. Sheldrick, D. Stalke, *J. Appl. Crystallogr.* **2015**, *48*, 3; b) APEX-IV (Version 4.0), Data Reduction and Frame Integration Programfor the CCD Area-Detector System, Bruker AXS Inc.: Madison, Wisconsin (USA), **2021**; c) M. Sevvana, M. Ruf, I. Usón, G. M. Sheldrick, R. Herbst-Irmer, *Acta Crystallogr.* **2019**, *D75*, 1040.
[27] G. M. Sheldrick, *Acta Crystallogr.* **2015**, *A71*, 3.
[28] G. M. Sheldrick, *Acta Crystallogr.* **2015**, *C71*, 3.
[29] O. V. Dolomanov, L. J. Bourhis, R. J. Gildea, J. A. K. Howard, H. Puschmann, *J. Appl. Crystallogr.* **2009**, *42*, 339.
[30] DIAMOND (Version 4.65), Crystal and Molecular Structure Visualization; Crystal Impact – Dr. H. Putz & Dr. K. Brandenburg GbR: Bonn (Germany), **2023**.
[31] OPUS (Version 7.5); Bruker Optik GmbH: Ettlingen (Germany), **2014**.
[32] OMNIC (Version 9.7.46); Thermo Fisher Scintific Inc.: Waltham, Massachusetts (USA), **2016**.
[33] ORIGINPRO (Version 9.9.0.220), Data Analysis and Graphing Software; OriginLab Corp.: Northampton, Massachusetts (USA), **2022**.
[34] S. Stoll, A. Schweiger, *J. Magn. Reson.* **2006**, *178*, 42.
[35] L. Bennett, B. Melchers, B. Proppe, *Freie Universität Berlin*, **2020**, published online, https://doi.org/10.17169/refubium-26754.
[36] a) H.-J. Werner, P. J. Knowles, G. Knizia, F. R. Manby, M. Schütz, *WIREs Comput. Mol. Sci.* **2012**, *2*, 242; b) H.-J. Werner, P. J. Knowles, F. R. Manby, J. A. Black, K. Doll, A. Heßelmann, D. Kats, A. Köhn, T. Korona, D. A. Kreplin, Q. Ma, T. F. Miller, III, A. Mitrushchenkov, K. A. Peterson, I. Polyak, G. Rauhut, M. Sibaev, *J. Chem. Phys.* **2020**, *152*, 144107; c) Molpro (Molpro 2021.3 and Molpro 2024.2), W. H.-J., P. Knowles, P. Celani, W. Györffy, A. Hesselmann, D. Kats, G. Knizia, A. Köhn, T. Korona, D. Kreplin, R. Lindh, Q. Ma, F. Manby, A. Mitrushenkov, G. Rauhut, M. Schütz, K. Shamasundar, T. Adler, R. Amos, J. Baker, S. Bennie, A. Bernhardsson, A. Berning, J. Black, P. Bygrave, R. Cimiraglia, D. Cooper, D. Coughtrie, M. Deegan, A. Dobbyn, K. Doll, M. Dornbach, F. Eckert, S. Erfort, E. Goll, C. Hampel, G. Hetzer, J. Hill, M. Hodges, T. Hrenar, G. Jansen, C. Köppl, C. Kollmar, S. Lee, Y. Liu, A. Lloyd, R. Mata, A. May, B. Mussard, S. McNicholas, W. Meyer, T. M. III, M. Mura, A. Nicklass, D. O'Neill, P. Palmieri, D. Peng, K. Peterson, K. Pflüger, R. Pitzer, I. Polyak, P. Pulay, M. Reiher, J. Richardson, J. Robinson, B. Schröder, M. Schwilk, T. Shiozaki, M. Sibaev, H. Stoll, A. Stone, R. Tarroni, T. Thorsteinsson, J. Toulouse, M. Wang, M. Welborn, B. Ziegler, **2021**.
[37] a) F. Neese, *WIREs Comput. Mol. Sci.* **2011**, *2*, 73; b) F. Neese, *WIREs Comput. Mol. Sci.* **2022**, *12*, e1606.
[38] Gaussian (Gaussian 16), M. J. Frisch, G. W. Trucks, H. B. Schlegel, G. E. Scuseria, M. A. Robb, J. R. Cheeseman, G. Scalmani, V. Barone, G. A.

© 2025 The Author(s). European Journal of Inorganic Chemistry published by Wiley-VCH GmbH

Petersson, H. Nakatsuji, X. Li, M. Caricato, A. V. Marenich, J. Bloino, B. G. Janesko, R. Gomperts, B. Mennucci, H. P. Hratchian, J. V. Ortiz, A. F. Izmaylov, J. L. Sonnenberg, Williams, F. Ding, F. Lipparini, F. Egidi, J. Goings, B. Peng, A. Petrone, T. Henderson, D. Ranasinghe, V. G. Zakrzewski, J. Gao, N. Rega, G. Zheng, W. Liang, M. Hada, M. Ehara, K. Toyota, R. Fukuda, J. Hasegawa, M. Ishida, T. Nakajima, Y. Honda, O. Kitao, H. Nakai, T. Vreven, K. Throssell, J. A. Montgomery Jr., J. E. Peralta, F. Ogliaro, M. J. Bearpark, J. J. Heyd, E. N. Brothers, K. N. Kudin, V. N. Staroverov, T. A. Keith, R. Kobayashi, J. Normand, K. Raghavachari, A. P. Rendell, J. C. Burant, S. S. Iyengar, J. Tomasi, M. Cossi, J. M. Millam, M. Klene, C. Adamo, R. Cammi, J. W. Ochterski, R. L. Martin, K. Morokuma, O. Farkas, J. B. Foresman, D. J. Fox, Wallingford, CT, **2016**.

[39] a) A. D. Becke, *Phys. Rev. A.* **1988**, *38*, 3098; b) C. Lee, W. Yang, R. G. Parr, *Phys. Rev. B* **1988**, *37*, 785; c) S. Grimme, J. Antony, S. Ehrlich, H. Krieg, *J. Chem. Phys.* **2010**, *132*, 154104; d) S. Grimme, S. Ehrlich, L. Goerigk, *J. Comput. Chem.* **2011**, *32*, 1456.

[40] E. Caldeweyher, S. Ehlert, A. Hansen, H. Neugebauer, S. Spicher, C. Bannwarth, S. Grimme, *J. Chem. Phys.* **2019**, *150*, 154122.

[41] a) G. D. Purvis, R. J. Bartlett, *J. Chem. Phys.* **1982**, *76*, 1910; b) K. Raghavachari, G. W. Trucks, J. A. Pople, M. Head-Gordon, *Chem. Phys. Lett.* **1989**, *157*, 479.

[42] a) P. J. Knowles, H.-J. Werner, *Chem. Phys. Lett.* **1985**, *115*, 259; b) H.-J. Werner, P. J. Knowles, *J. Chem. Phys.* **1985**, *82*, 5053.

[43] a) E. R. Davidson, D. W. Silver, *Chem. Phys. Lett.* **1977**, *52*, 403; b) H. J. Werner, P. J. Knowles, *J. Chem. Phys.* **1988**, *89*, 5803; c) P. J. Knowles, H. J. Werner, *Chem. Phys. Lett.* **1988**, *145*, 514.

[44] S. Grimme, A. Hansen, S. Ehlert, J.-M. Mewes, *J. Chem. Phys.* **2021**, *154*, 064103.

[45] a) F. Neese, *Chem. Phys. Lett.* **2000**, *325*, 93; b) C. Kollmar, K. Sivalingam, B. Helmich-Paris, C. Angeli, F. Neese, *J. Comput. Chem.* **2019**, *40*, 1463; c) C. Kollmar, K. Sivalingam, F. Neese, *J. Chem. Phys.* **2020**, *152*, 214110; d) C. Kollmar, K. Sivalingam, Y. Guo, F. Neese, *J. Chem. Phys.* **2021**, *155*, 234104; e) M. Ugandi, M. Roemelt, *Int. J. Quantum Chem.* **2023**, *123*, e27045.

[46] W. J. Hehre, R. Ditchfield, J. A. Pople, *J. Chem. Phys.* **1972**, *56*, 2257.

[47] F. Neese, E. F. Valeev, *J. Chem. Theory Comput.* **2011**, *7*, 33.

[48] R. A. Kendall, T. H. Dunning, R. J. Harrison, *J. Chem. Phys.* **1992**, *96*, 6796.

[49] a) J. G. Hill, K. A. Peterson, *J. Chem. Phys.* **2017**, *147*, 244106; b) K. A. Peterson, T. H. Dunning Jr., *J. Chem. Phys.* **2002**, *117*, 10548.

[50] S. Grimme, C. Bannwarth, P. Shushkov, *J. Chem. Theory Comput.* **2017**, *13*, 1989.

[51] Chemcraft (CHEMCRAFT 1.8), G. A. Zhurko, Ivanovo (Russia), **2005**.

[52] P. R. Spackman, M. J. Turner, J. J. McKinnon, S. K. Wolff, D. J. Grimwood, D. Jayatilaka, M. A. Spackman, *J. Appl. Crystallogr.* **2021**, *54*, 1006.

[53] W. Humphrey, A. Dalke, K. Schulten, *J. Mol. Graphics* **1996**, *14*, 33.

[54] a) D. T. Sawyer, T. S. Calderwood, K. Yamaguchi, C. T. Angelis, *Inorg. Chem.* **1983**, *22*, 2577; b) K. Yamaguchi, T. S. Calderwood, D. T. Sawyer, *Inorg. Chem.* **1986**, *25*, 1289.

[55] a) W. Schnick, M. Jansen, *Angew. Chem. Int. Ed.* **1985**, *24*, 54; b) W. Schnick, M. Jansen, *Angew. Chem.* **1985**, *97*, 48.

[56] F. Gu, H. Dong, Y. Li, Z. Sun, F. Yan, *Macromolecules* **2014**, *47*, 6740.

[57] S. C. Abrahams, J. Kalnajs, *Acta Crystallogr.* **1955**, *8*, 503.

[58] X. Tao, C. G. Daniliuc, O. Janka, R. Pöttgen, R. Knitsch, M. R. Hansen, H. Eckert, M. Lübbesmeyer, A. Studer, G. Kehr, G. Erker, *Angew. Chem. Int. Ed.* **2017**, *56*, 16641.

[59] R. Huacuja, D. J. Graham, C. M. Fafard, C.-H. Chen, B. M. Foxman, D. E. Herbert, G. Alliger, C. M. Thomas, O. V. Ozerov, *J. Am. Chem. Soc.* **2011**, *133*, 3820.

[60] D. D. Dexter, C. N. Sutherby, M. W. Grieb, R. C. Beaumont, *Inorg. Chim. Acta* **1984**, *86*, 19.

[61] A. Bakac, I. A. Guzei, *Inorg. Chem.* **2000**, *39*, 736.

[62] J. Cho, J. Woo, W. Nam, *J. Am. Chem. Soc.* **2010**, *132*, 5958.

[63] S. Hong, K. D. Sutherlin, J. Park, E. Kwon, M. A. Siegler, E. I. Solomon, W. Nam, *Nat. Commun.* **2014**, *5*, 5440.

[64] F. Schax, S. Suhr, E. Bill, B. Braun, C. Herwig, C. Limberg, *Angew. Chem. Int. Ed.* **2015**, *54*, 1352.

[65] K. Qin, C. D. Incarvito, A. L. Rheingold, K. H. Theopold, *Angew. Chem. Int. Ed.* **2002**, *41*, 2333.

[66] M.-L. Wind, B. Braun-Cula, F. Schax, C. Herwig, C. Limberg, *Isr. J. Chem.* **2020**, *60*, 1057.

[67] F. Oddon, Y. Chiba, J. Nakazawa, T. Ohta, T. Ogura, S. Hikichi, *Angew. Chem. Int. Ed.* **2015**, *54*, 7336.

[68] M.-L. Wind, S. Hoof, C. Herwig, B. Braun-Cula, C. Limberg, *Chem. Eur. J.* **2019**, *25*, 5743.

[69] C. Würtele, E. Gaoutchenova, K. Harms, M. C. Holthausen, J. Sundermeyer, S. Schindler, *Angew. Chem. Int. Ed.* **2006**, *45*, 3867.

[70] K. Fujisawa, M. Tanaka, Y. Moro-oka, N. Kitajima, *J. Am. Chem. Soc.* **1994**, *116*, 12079.

[71] A. Brinkmeier, R. A. Schulz, M. Buchhorn, C.-J. Spyra, S. Dechert, S. Demeshko, V. Krewald, F. Meyer, *J. Am. Chem. Soc.* **2021**, *143*, 10361.

[72] X. Zhang, G. R. Loppnow, R. McDonald, J. Takats, *J. Am. Chem. Soc.* **1995**, *117*, 7828.

[73] D. R. Lide, *CRC Handbook of Chemistry and Physics. A Ready-Reference Book of Chemical and Physical Data*, 85th ed., CRCPress, Boca Raton, FL, **2004**.

[74] W. Klein, M. Jansen, *Z. Naturforsch. B* **1999**, *54*, 1345.

[75] N. Korber, M. Jansen, *Chem. Ber.* **1996**, *129*, 773.

[76] W. Schnick, M. Jansen, *Rev. Chim. Miner.* **1987**, *24*, 446.

[77] T. Kellersohn, N. Korber, M. Jansen, *J. Am. Chem. Soc.* **1993**, *115*, 11254.

[78] H. Nuss, M. Jansen, *Z. Naturforsch. B* **2009**, *64*, 1325.

[79] N. Korber, M. Jansen, *J. Chem. Soc. Chem. Commun.* **1990**, 1654.

[80] M. Jansen, W. Hesse, *Z. Anorg. Allg. Chem.* **1988**, *560*, 47.

[81] W. Klein, M. Jansen, *Z. Anorg. Allg. Chem.* **2000**, *626*, 947.

[82] W. Klein, M. Jansen, *Z. Naturforsch. B* **2005**, *60*, 426.

[83] W. Hesse, M. Jansen, *Angew. Chem. Int. Ed.* **1988**, *27*, 1341.

[84] W. Assenmacher, M. Jansen, *Z. Anorg. Allg. Chem.* **1995**, *621*, 431.

[85] a) H. Seyeda, M. Jansen, *Z. Kristallogr. New Cryst. Struct.* **1997**, *212*, 233; b) W. Assenmacher, M. Jansen, *Z. Kristallogr. Cryst. Mater.* **1995**, *210*, 704.

[86] H. Seyeda, K. Armbruster, M. Jansen, *Chem. Ber.* **1996**, *129*, 997.

[87] J. R. Schmid, O. R. H. Rennefeld, A. Wiesner, M. Jansen, S. Riedel, *Chem. Eur. J.* **2024**, *30*, e202400585.

[88] W. Klein, M. Jansen, *Z. Naturforsch. B* **2001**, *56*, 287.

[89] R. Marx, R. M. Ibberson, *Solid State Sci.* **2001**, *3*, 195.

[90] L. P. Viegas, A. J. C. Varandas, *J. Chem. Theory Comput.* **2010**, *6*, 412.

[91] L. A. Burns, Á. V. Mayagoitia, B. G. Sumpter, C. D. Sherrill, *J. Chem. Phys.* **2011**, *134*, 084107.

[92] L. Rao, H. Ke, G. Fu, X. Xu, Y. Yan, *J. Chem. Theory Comput.* **2009**, *5*, 86.

[93] a) T. Lu, F. Chen, *J. Comput. Chem.* **2012**, *33*, 580; b) T. Lu, *J. Chem. Phys.* **2024**, *161*, 082503.

[94] P. Borowski, B. O. Roos, S. C. Racine, T. J. Lee, S. Carter, *J. Chem. Phys.* **1995**, *103*, 266.

[95] F. Kleemiss, O. V. Dolomanov, M. Bodensteiner, N. Peyerimhoff, L. Midgley, L. J. Bourhis, A. Genoni, L. A. Malaspina, D. Jayatilaka, J. L. Spencer, F. White, B. Grundkötter-Stock, S. Steinhauer, D. Lentz, H. Puschmann, S. Grabowsky, *Chem. Sci.* **2021**, *12*, 1675.

[96] W. Schnick, *Ph.D. Thesis*, Univ. Hannover **1986**.

[97] D. W. Arnold, C. S. Xu, E. H. Kim, D. M. Neumark, *J. Chem. Phys.* **1994**, *101*, 912.

Manuscript received: January 21, 2025
Revised manuscript received: March 2, 2025
Accepted manuscript online: March 4, 2025
Version of record online: March 21, 2025

© 2025 The Author(s). European Journal of Inorganic Chemistry published by Wiley-VCH GmbH